Marine and Petroleum Geology 145 (2022) 105872

Contents lists available at ScienceDirect

Marine and Petroleum Geology

journal homepage: www.elsevier.com/locate/marpetgeo

High resolution Late Miocene sediment accommodation rates and subsidence history in the Austrian part of the Vienna Basin

Mathias Harzhauser [a,*], Matthias Kranner [a], Oleg Mandic [a], Stjepan Ćorić [b], Wolfgang Siedl [c]

[a] Geological-Paleontological Department, Natural History Museum Vienna, Burgring 7, 1010, Vienna, Austria
[b] Geological Survey Austria, Neulinggasse 38, 1030, Vienna, Austria
[c] OMV E&P GmbH, Trabrennstraße 6-8, 1020, Vienna, Austria

ARTICLE INFO

Keywords:
Vienna basin
Well log correlation
Subsidence history
Sedimentation rates
Miocene
Lake Pannon

ABSTRACT

We present the first detailed intra-basin correlation of Upper Miocene deposits in the Austrian part of the Vienna Basin (VB) integrating the most important hydrocarbon fields. Herein, we use a high resolution dataset by separating the Pannonian (= Tortonian) stack into 20 lithostratigraphic units, which allow calculating regional differences in sedimentation rates over a time span of ~1.6 Ma. During this time span we recognize an initial phase of high lateral variability in thicknesses, reflecting the influence of paleo-topography on deposition during the early Pannonian. The relief difference of about 300 m was rapidly filled by lake marls and delta lobes of the Paleo-Danube. Subsequently, lateral variability in sediment thicknesses declined strongly around 11.0 Ma. At that point the relief was largely sealed, and subsidence became the controlling factor. Our data document a shift of high subsidence rates from the southern VB to the northern VB into three steps, initiated by increased activity of the Steinberg Fault around 10.5–10.4 Ma. Sedimentation rates have been declining during the early Pannonian but reveal a strong pulse in subsidence during the middle Pannonian. The still high sedimentation rates during the late Pannonian indicate persisting extensional tectonics in the VB throughout the Late Miocene and question the prevailing tectonic model of a compressional regime for this time. The lack of uppermost Pannonian deposits in most wells documents a post-Pannonian erosion of about 400 m in large parts of the VB.

1. Introduction

The Vienna Basin (VB) formed at the Alpine–Carpathian junction during the Neogene and underwent a complex tectonic history. The about 200 km long and 60 km wide basin is interpreted as extensional basin, initiated by lateral extrusion of the Eastern Alps (Decker et al., 2005; Hinsch et al., 2005; Siedl et al., 2020). The frequently cited pull-apart mechanism as proposed by Royden (1985) was not supported by seismic data (Siedl et al., 2020). The basin is composed of several horst and graben structures forming different subbasins (Fig. 1), each with its own geodynamic evolution and deviating paleobathymetric developments during the Miocene. The Miocene tectonic subsidence evolution of the VB has been discussed in detail by Hölzel et al. (2008) and Lee and Wagreich (2016, 2017). Kranner et al. (2021) analyzed the paleobathymetric development during the marine phases of the VB from the Lower Miocene Ottnangian to the Middle Miocene Sarmatian but not for the Upper Miocene due to the lack of foraminifers. The Upper Miocene Pannonian deposits correspond to the Tortonian of the standard chronostratigraphy (Fig. 2) and have been integrated also by Hölzel et al. (2008) and Lee and Wagreich (2016, 2017) in their analyses. These authors focused on the change of the tectonic regime from piggyback basin to extensional systems during the Early and Middle Miocene.

The Pannonian deposits of the Vienna Basin reflect a broad range of depositional environments ranging from beach ridges, sandwaves, river channels, delta lobes to deep lacustrine offshore marls (Kováč et al., 1998; Harzhauser et al., 2003, 2004; Borzi et al., 2022). The rapid endemic evolution of its mollusc fauna allows for a detailed biostratigraphic subdivision of Pannonian strata (Papp, 1951; Magyar et al., 1999a, 1999b; Magyar, 2021). Harzhauser et al. (2004) correlated the letter zones of Papp (1951) (Zones A to H) with lithological units in wells Gösting 4 and Eichhorn 1 and subdivided these according to well log patterns. This scheme is applied herein to resolve and correlate a large part of the Pannonian strata spanning for the first time parts of the northern, central and northern part of the southern VB (Fig. 1).

* Corresponding author.
E-mail addresses: mathias.harzhauser@nhm-wien.ac.at (M. Harzhauser), matthias.kranner@nhm-wien.ac.at (M. Kranner), oleg-mandic@nhm-wien.ac.at (O. Mandic), stjepan.coric@geologie.ac.at (S. Ćorić), wolfgang.siedl@omv.com (W. Siedl).

https://doi.org/10.1016/j.marpetgeo.2022.105872
Received 26 May 2022; Received in revised form 5 August 2022; Accepted 6 August 2022
Available online 19 August 2022

Cross-correlations of well logs in the VB are hampered by the different tectonic settings in the various subbasins during the Early Miocene and most of the Middle Miocene (Kranner et al., 2021). This situation changed with the Sarmatian when well log patterns can be correlated across large parts of the then shallow basin (Harzhauser and Piller, 2004a, 2004b). These studies showed, that the Upper Miocene is better suited for these correlations as the influence of faults was weaker then compared the early to middle Miocene. Consequently, the well logs display similar patterns throughout the VB.

Little is known about the Late Miocene tectonic regime in the VB. This study tries to get a better understanding by using well log correlation. Our work aims for integrating wells from the most important hydrocarbon production fields in the Austrian part of the VB to detect lateral changes in sediment thickness. These data are transferred into sedimentation rates to trace regional differences in subsidence across an about 100-km-long NE–SW trending transect. This on its turn will provide new information on the tectonic evolution of the VB.

2. Geological setting

The Pannonian succession of the Vienna Basin is divided into the lacustrine Bzenec Formation, which is linked to Lake Pannon, and the Cary and Gbely formations, which formed in floodplain environments (Čtyroký, 2000; Harzhauser et al., 2004) (Fig. 2). A biostratigraphic zonation of the Pannonian of the Vienna Basin was developed by Papp (1951), who used letters for the zones. The Bzenec Formation comprises the lower Pannonian units A to C of Papp (1951) and the middle Pannonian units D and E of Papp (1951) (units A–E in Figs. 2, 3–6). The Cary Formation corresponds to unit F of Papp (1951) and the Gbely Formation covers the units G and H of Papp (1951). Sedimentation was continuous from units A to F. A hiatus might separate the Cary Formation from the Gbely Formation based on biostratigraphic data (Harzhauser et al., 2004) but seismic data are too poor for these shallow units to detect erosional features (Fig. 7B).

The Bernhardsthal and Rabensburg fields are the northernmost hydrocarbon production areas in the investigation area (Fig. 1). They are bound in the west by the Steinberg Fault and by the Eichhorn-Rabensburg High in the east. Wells are partly positioned on an uplifted block (e.g., Bernhardsthal 5, 6, 7, Rabensburg 2) and partly on a downthrown block (e.g., Rabensburg 11, Paltendorf 1, T1) (Figs. 3 and 7A). The Zistersdorf Depression and the Moravian Central Depression form major depocenters in this region. The Steinberg Fault is also the

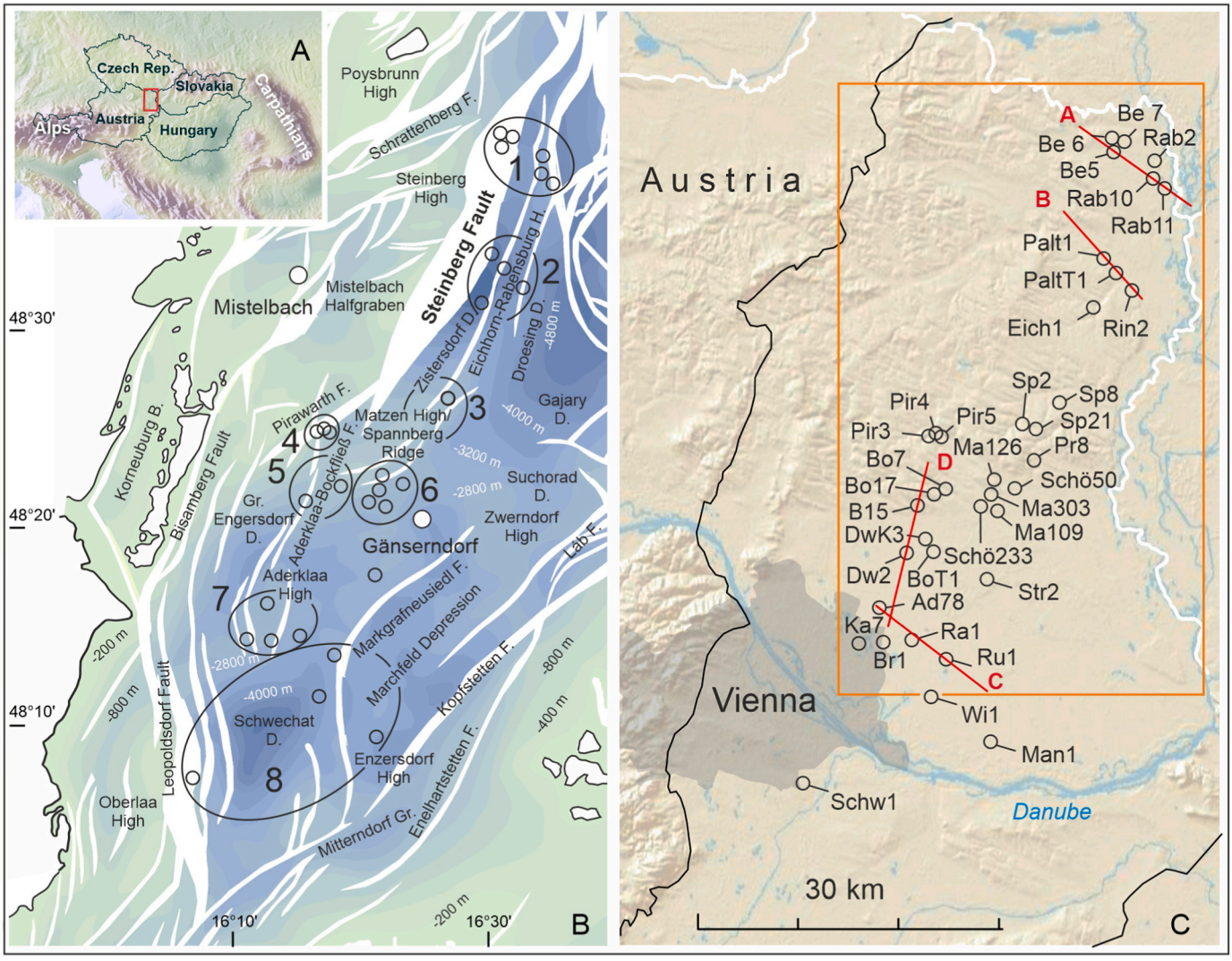

Fig. 1. A. Location of the Vienna Basin within central Europe. **B.** Tectonic setting of the central and northern Vienna Basin modified after Harzhauser et al. (2020) (B: basin, D: depression, F: fault, H: high; 1: Bernhardsthal-Rabensburg field, 2: Paltendorf field, 3: Spannberg field, 4: Pirawarth field, 5: Bockflieβ field, 6: Matzen field, 7: Aderklaa field, 8: Schwechat field). **C.** Topographic map of the Vienna Basin (white lines represent borders between countries) with the positions of the investigated wells (open circles with well acronyms), red lines represent seismic lines illustrated in Fig. 7 (lines A–C) and Fig. 8 (line D). Orange square shows extension of the Vienna Basin Super Merge 3D survey. (For interpretation of the references to colour in this figure legend, the reader is referred to the Web version of this article.)

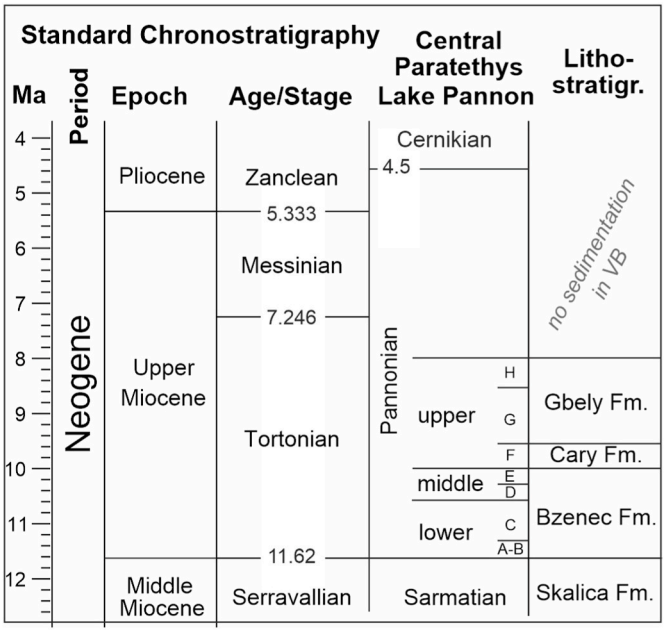

Fig. 2. Stratigraphic table showing the correlation of the regional stages and the lithostratigraphic units (after Gradstein et al., 2020; Harzhauser et al., 2004; Mandic et al., 2015).

western border of the Paltendorf field, which is internally structured by the Zistersdorf and the Droesing depressions and the Eichhorn-Rabensburg Horst. The Spannberg and Pirawarth fields are situated north of the Spannberg Ridge and the Matzen High. The area is bounded to the NW by the Pirawarth Fault. South of the Matzen High and the Spannberg Ridge follow the Bockfließ, Matzen and Aderklaa fields. Their western border is formed by the Aderklaa-Bockfließ Fault. The Aderklaa High forms an important high zone. The Schwechat field is the southernmost investigated region and is characterized by the Schwechat Depression. Its western boundary is formed by the Leopoldsdorf Fault and the Oberlaa High. To the east, the Schwechat Depression is bounded by the Markgrafneusiedl Fault and the Enzersdorf High.

3. Material and methods

3.1. Well logs

The company OMV provided well log data for Resistivity (RES), Spontaneous Potential (SP) and Gamma Radiation (GR) for Pannonian strata of 36 wells with a sample resolution of about 15 cm (Figs. 3–6). The selected wells cover a roughly NE-SW trending cross-section through the Austrian part of the VB, crossing several of the most important hydrocarbon production fields (Fig. 1); see Kranner et al. (2021) for descriptions of the fields). Table 1 provides the acronyms of the wells and lists the thicknesses for the Pannonian units. Quaternary deposits have not been distinguished because these are not well constrained in the wells due to their minor thickness. Thus, the thickness of the uppermost unit in each well may be slightly uncertain.

The resistivity log is an electrical well log, which reflect the resistivity of the drilled sediments and is measured in ohm-meter (Ωm).

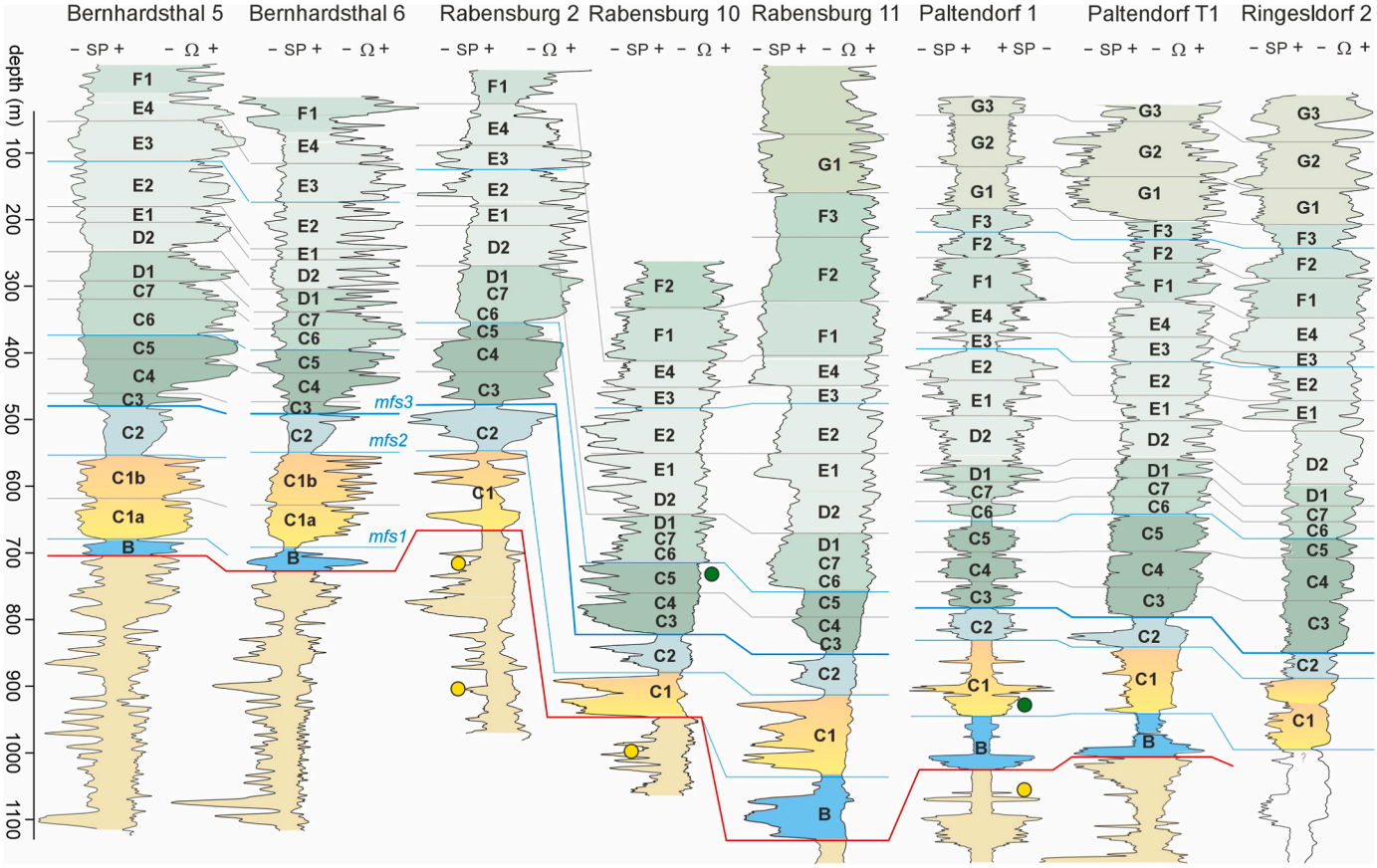

Fig. 3. Correlation of well logs of the Bernhardsthal, Rabensburg and Paltendorf fields (A to G3 represent Pannonian units). Circles indicate position of samples for biostratigraphy (green = Pannonian, yellow = Sarmatian, white = barren sample). Red line = sequence boundary between Sarmatian and Pannonian strata. Blue lines represent major flooding surfaces. (For interpretation of the references to colour in this figure legend, the reader is referred to the Web version of this article.)

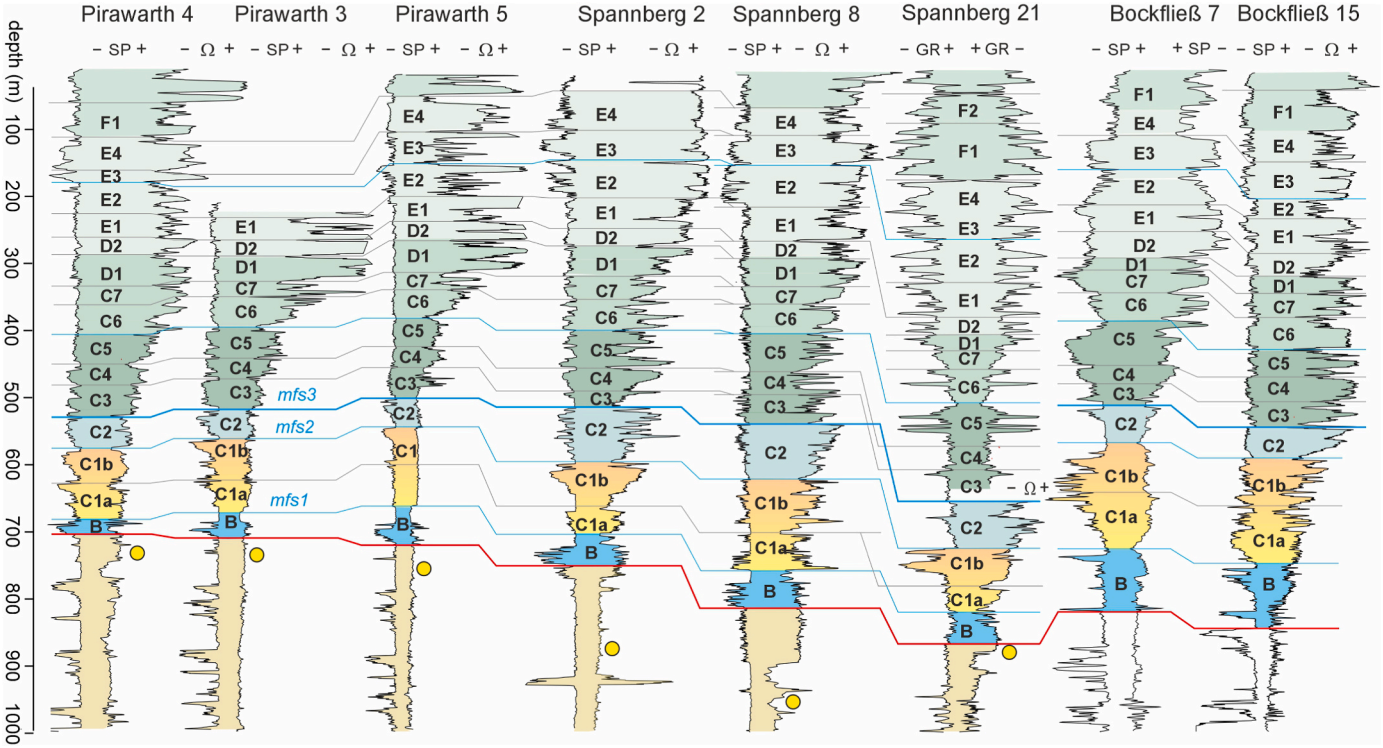

Fig. 4. Correlation of well logs in the Pirawarth, Spannberg and Bockflieβ fields. Colors and symbols as in Fig. 3. (For interpretation of the references to colour in this figure legend, the reader is referred to the Web version of this article.)

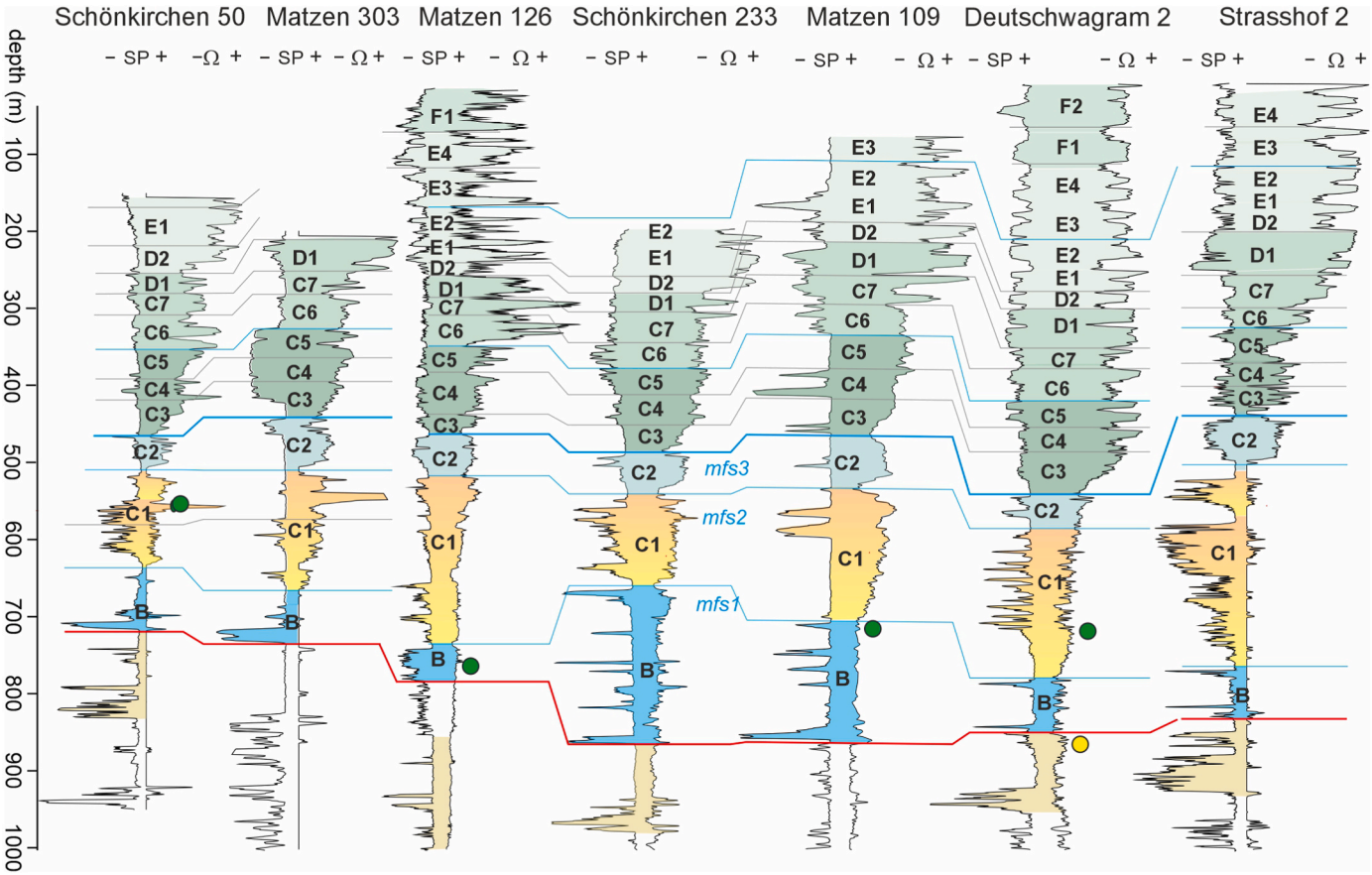

Fig. 5. Correlation of well logs in the Matzen field. Colors and symbols as in Fig. 3. (For interpretation of the references to colour in this figure legend, the reader is referred to the Web version of this article.)

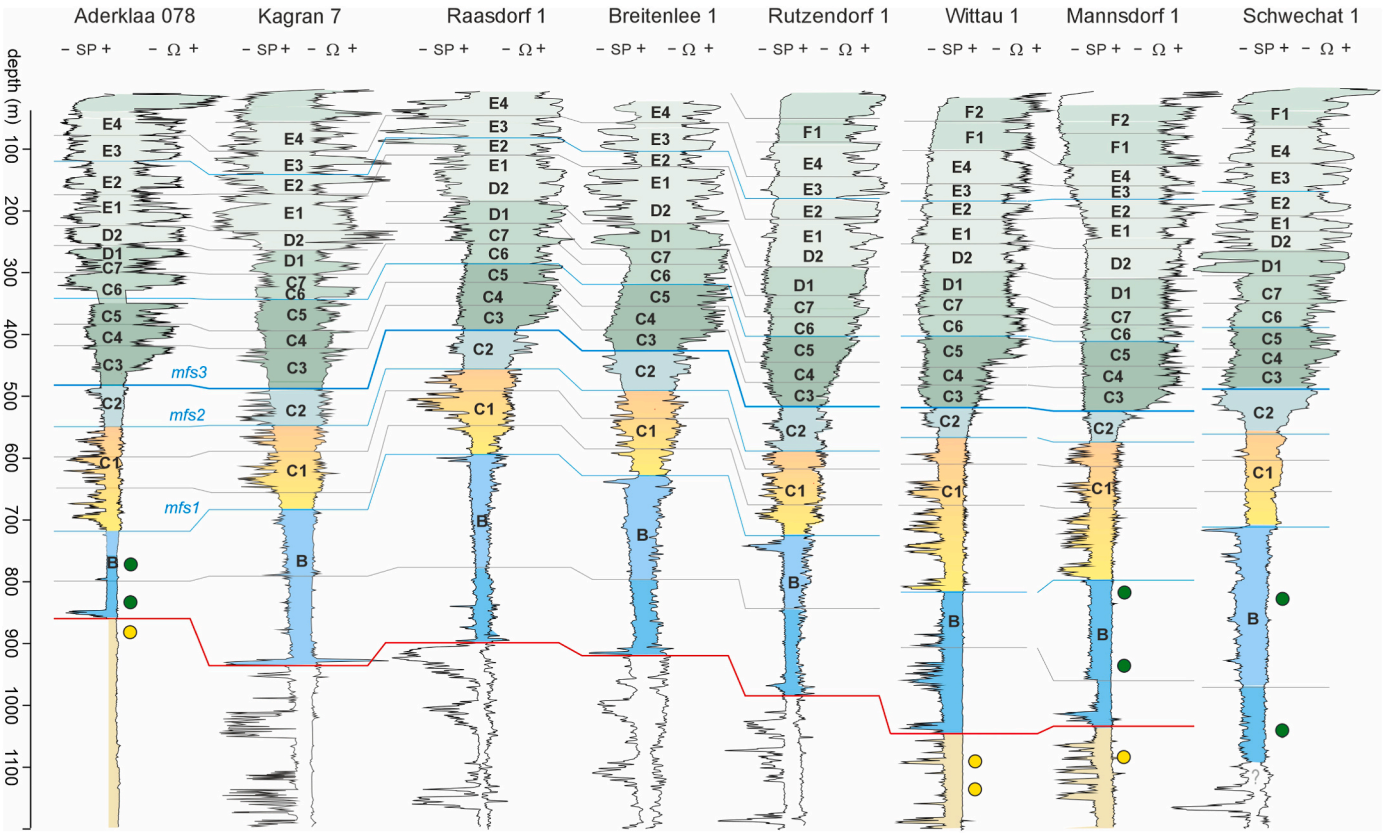

Fig. 6. Correlation of well logs in the Aderklaa and Schwechat fields. Colors and symbols as in Fig. 3. (For interpretation of the references to colour in this figure legend, the reader is referred to the Web version of this article.)

Resistivity is generally high in sandstones and comparatively low in shales (Evenick, 2008). The spontaneous potential log measures the natural or spontaneous potential difference between the given depth in the borehole and the surface in millivolts. The SP log has no absolute scale and only relative changes in the SP values are relevant. The SP log is often read against the shale base line, which is defined by the highest SP values in impermeable shales (right side in the illustrated SP logs). This is opposed by the sand line with the lowest SP signals in clean sands (left side in the illustrated SP logs). Gamma radiation is available only for well Spannberg 21. Gamma radiation in well logs is mainly based on the presence of potassium 40, uranium, and thorium. In sedimentary facies, these elements are often associated with clays and these sediments will generally have a higher GR signal than sand and gravel. The presence of fresh/salt water and the presence of hydrocarbons may complicate these rule-of-thumbs interpretations of RES and SP logs. Nevertheless, the lithologies of the numerous cores that have been drilled in the VB proof that high RES/low SP values indicate sand and gravel whereas low RES/high SP values correspond to clay and marl successions (see Asquith et al., 2004 and Evenick, 2008 for an in-depth discussion on electro logs). The investigated well logs display characteristic successions of high/low SP/RES values, with characteristic shale line intervals, which allow for an intra-basin correlation as presented in Figs. 3–6. These shale line intervals represent flooding surfaces, which are basin-wide phenomena. In addition, we use a subdivision of the logs (units A–G), which corresponds to the terminology of Papp (1951) and Harzhauser et al. (2004).

Sediment thickness of the units is measured along the wells assuming vertical wells. In some cases, units are incomplete due to synsedimentary erosion. The full data set on thicknesses of units in the investigated wells is given in Table 1.

3.2. Seismic data

A 3D seismic survey is available for the entire region. Seismic data of several seismic vintages (1994–2013) were merged to an approximately 1800 km^2 seismic survey called Vienna Basin Super Merge (VBSM). The extension of the VBSM is shown in Fig. 1. Seismic processing was performed by OMV in-house between May 2012 and February 2014. For details on the VBSM and numerous 2D cross-sections see Siedl et al. (2020). Seismic allows for cross-correlation within hydrocarbon fields but in many cases strong tectonic deformation hampers a straightforward correlation of horizons between uplifted and downthrown blocks (see Fig. 7). Moreover, the seismic resolution for the uppermost 200 m is very poor, because the seismic survey focused on deeper strata. Therefore, especially the Cary and Gbely formations are not well resolved by seismics and the interpretation relies mainly on well logs.

The sediment thicknesses have not been corrected for compaction, because no porosity data are available. Thus, the calculated vertical thickness is based on the in situ (gravitational compacted) thickness and do not represent the paleo-thickness. Consequently, the calculated sedimentation rates have to be read as underestimations.

3.3. Biostratigraphic data

55 samples have been taken from cores in the core-shed in Gänserndorf (Austria) for micropaleontological analysis and for the detection of macrofossils. All samples were treated with diluted H_2O_2 (12%) for several hours and sieved with tap water through a standard set of sieves (500, 250, 125 and 63 μm) and later on oven dried at 40 °C. 10 samples have been analyzed for Calcareous Nannoplankton. All samples were treated for few seconds in an ultrasonic bath. Afterwards smear slides were made drying few drops of suspension on the object glass and fixed using Canada balsam. All smear slides were investigated with a

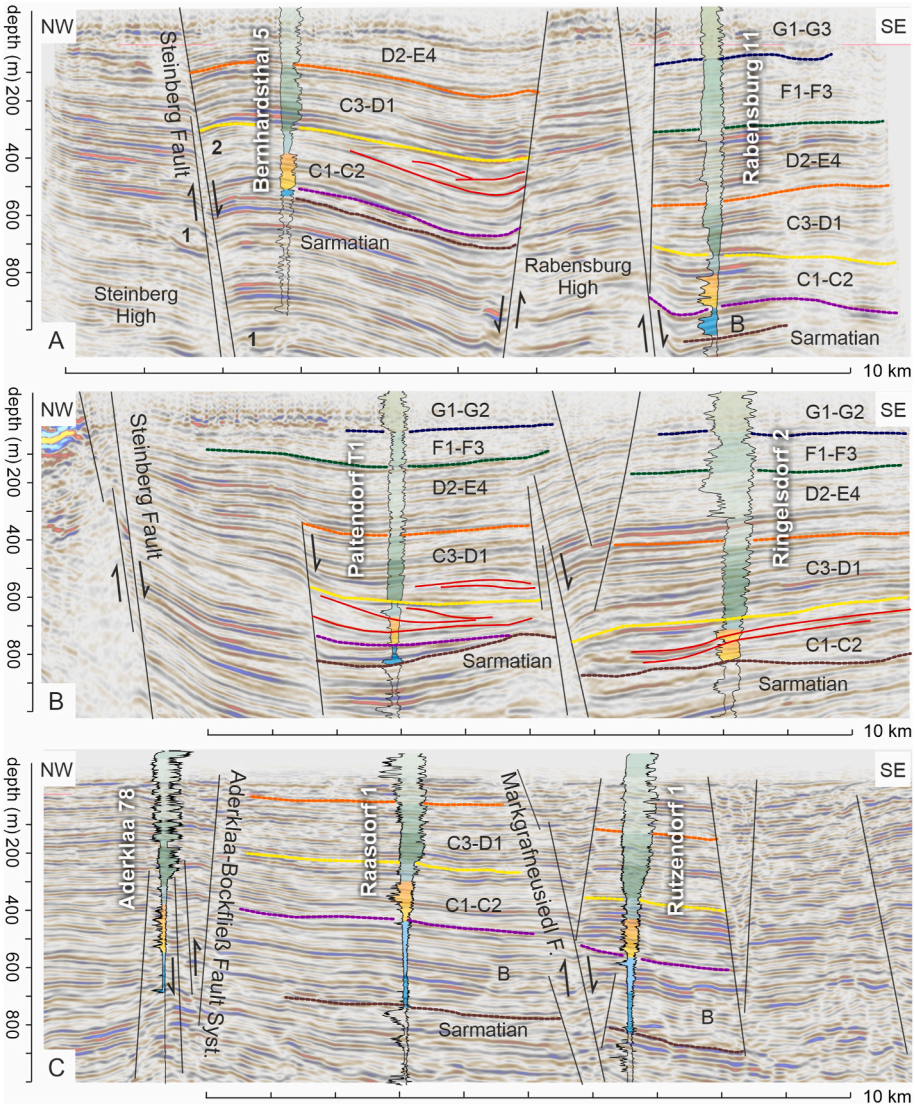

Fig. 7. Seismic lines showing Pannonian strata and representative wells in the Bernhardsthal-Rabensburg field (A), the Paltendorf field (B) and Aderklaa field (C); see Fig. 1 for geographic position of seismic lines. Red lines indicate deltaic bodies. 1: Sarmatian incised valley separated by Steinberg Fault; 2: rollover anticline. (For interpretation of the references to colour in this figure legend, the reader is referred to the Web version of this article.)

Leica microscope with 1000 magnification. The identified foraminifers and molluscs are given in appendix 1 (barren samples are not shown); data on calcareous nannoplankton are given in appendix 2.

All statistical analyses were performed with the software PAST version 4.05 (Hammer et al., 2001).

4. Results

4.1. Well log correlations

The position of Sarmatian/Pannonian boundary was defined in previous projects (e.g. Harzhauser et al., 2004; Borzi et al., 2022) based on the disappearance of marine fossils and the appearance of lacustrine ostracods and molluscs.

Units A–B: The boundary is often indicated by a short interval of high amplitude RES values of up to about 20 m (basal part of blue unit in Figs. 3–6). This unit corresponds to unit A of Harzhauser et al. (2004) and can be identified easily, where it overlies Sarmatian shale line logs (e.g., Matzen 303, Schönkirchen 233) but is difficult to detect where it follows Sarmatian channel fills (e.g., Strasshof 2, Raasdorf 1). In these cases, we include unit A in unit B. This unit is well developed in southern wells but is absent in northern wells. The boundary between the Sarmatian and Pannonian deposits corresponds to the sequence boundary SB1 of Borzi et al. (2022).

Unit A is followed by a unit of low RES and SP values, corresponding to zone B of Papp (1951) and unit B of Harzhauser et al. (2004). Unit B is very variable in thickness. In northern fields, it attains only few tens of meters of thickness (e.g., Bernhardsthal wells, Fig. 3) or may even be missing (Rab 2, Rab 10). It is more prominent in the Paltendorf field (m = 85 m, σ = 25.7 m) (Fig. 3), slightly thinner again in the Pirawarth, Spannberg and Bockfließ fields (m = 59 m; σ = 23.5 m) (Figs. 4 and 8) and increases rapidly from the Matzen field (m = 78 m, σ = 36.8 m) (Fig. 5), via the Aderklaa field (m = 256 m, σ = 78.3 m) (Figs. 6 and 7C) to the Schwechat field (m = 262 m, σ = 111.4 m) (Fig. 7). Especially in the southern part of the basin this unit has a characteristic shale line appearance (e.g., Raasdorf 1, Breitenlee 1, Rutzendorf 1) and is subdivided there by a flooding surface (Fig. 6). In northern wells, this unit displays also high amplitude RES values.

Units C–D1: A short but marked shale line interval separates unit B from unit C1, corresponding to a major flooding surface (= mfs 1 in Borzi et al., 2022). Above this marker bed follows an up to 260-m-thick unit of funnel-shaped or blocky RES and SP logs, characterized by high

frequency and high amplitude RES values typically mirrored by SP logs with lower amplitude fluctuations. Unit C1 has an average thickness of 147 m (σ = 43.1 m) and displays a slight NE-SW trend towards a higher thickness with a maximum in the Aderklaa and Schwechat fields (262 m in Strasshof 2) (Fig. 6). Unit C2 is bracketed by two marked flooding surfaces and represents a single funnel-to serrated cylinder-shaped unit often with coarsening upwards trend. Its mean thickness ranges around 60 m with moderate variability (σ = 14.0 m). Its lowest thickness of about 45 m is developed in the Paltendorf and Pirawarth fields but no thickness trend was established. Units C3 to C5 comprises about five to six, serrated, funnel-shaped sequences with distinct coarsening upwards trends and high RES values. The sequences often form three more distinct units (e.g., Paltendorf 1, Pirawarth 3, Bockflieβ 15, Aderklaa 78) but may be largely amalgamated into a serrated cylinder-shaped succession especially in the southern wells (e.g., Rutzendorf 1, Mannsdorf 1) (Fig. 6). In some wells, the SP-log of unit C5 is vaguely bell shaped (e.g., Bockflieβ 7, Bockflieβ 17, Kagran 7) (Fig. 6). The thickness of C3, C4, C5 ranges around 42 m, 36 m and 45 m on average with a standard deviation of 10–12 m. The merged thickness of all three units does not show a general trend but a slightly higher thickness is observed in the Paltendorf Field. Another flooding surface separates units C3–C5 from units C6–D2, which again comprise a succession of broad, funnel-shaped to barrel-shaped sequences. These are often well separated into three to four units by short high SP/low RES intervals forming a distinct serration (e.g., Aderklaa 78, Deutschwagram 2) (Figs. 5 and 6) but may form blocky, amalgamated units in southern wells (e.g., Rutzendorf 1, Wittau 1, Mannsdorf 1) (Fig. 6). Individual units display a similar average thickness (C6 = 38 m, C7 = 31 m, D1 = 37 m) and a comparable variability in thickness (σ = 8–14 m). The thickness of units C6–D1 is rather constant across most of the fields except for the Rabensburg and Paltendorf fields with a distinctly lower thickness.

Units D2–E: Units D1, E1, E2, E3 and E4 are characterized by funnel-to serrated cylinder-shaped sequences with high RES and low SP amplitudes. These units are often blocky and amalgamated, thus complicating cross-correlations, but may also form well separated funnel-shapes sequences (e.g., Eichhorn 1, Spannberg 21) (Figs. 4 and 5). The average thickness is similar for all five units (D2 = 40 m, E1 = 44 m, E2 = 48 m, E3 = 42 m, E4 = 50 m) with a standard deviation around 12–16 m. Unit D2 attains its maximum thickness in the Bernhardsthal and Rabensburg and Paltendorf fields and becomes thinner towards the south. Similarly, unit E2 displays an overall NE-SW trend towards a lower thickness with a drop in the Bockflieβ region, which is also evident for unit E4. Consequently, the entire package of units D2 to E4 shows a clear trend from a higher thickness of about 250 m in the Bernhardsthal, Rabensburg and Paltendorf fields via an intermediate thickness of 213 m in the Pirawarth, Spannberg, Bockflieβ fields to a slightly lower thickness of about 200 m in the Matzen, Aderklaa and Schwechat fields.

Unit F: Units F1 and F2 represent serrated bell-shaped curves (e.g., Paltendorf 1, Ringelsdorf 2, Spannberg 21, Deutschwagram 2) followed by a moderately funnel-to cylinder-shaped unit F3 (e.g., Rabensburg 11, Ringelsdorf 2). Whilst unit F1 is present in all fields, units F2 and F3 have a restricted distribution and F3 is limited to the Rabensburg and Paltendorf fields (Fig. 3). The average thickness of F1 is 61 m, 57 m for F2 and 53 m for F3 with a standard deviation around 13 m (F1) and 21–23 m (F2, F3). Unit F1 displays a slight NE-SW trend of decreasing thickness and unit F2, too, shows a distinct decrease in thickness from the Rabensburg and Paltendorf fields towards the more southern fields.

Unit G: The topmost units G1, G2 and G3 are only documented from Rabensburg 11, Paltendorf 1, Paltendorf T1 and Ringelsdorf 2 (Fig. 3). These units are moderately serrated cylinder-shaped to vaguely bell-shaped and attain about 69 m (G1; σ = 13.2 m) and 80 m (G2, σ = 10.0 m) in thickness. Unit G3 is incomplete in all available records but attains at least 70 m in thickness. Seismic data of Borzi et al. (2022) document the presence of deltaic bodies in the lower Pannonian and a decreasing occurrence of clinoforms thereafter (Fig. 7). Instead, continuous reflectors predominate in the middle and upper Pannonian (Figs. 7 and 8). Fault related differences in sediment thickness were detected by Borzi et al. (2022) within the deltaic bodies mainly along the Steinberg Fault System along the northwestern margin of the VB. These faults, however, did not play a role for the herein observed trends.

The trends in sediment thickness for most units can only be documented from well data, first, because the resolution of the seismic data does not capture these differences reliably and second, because the faults make it difficult to trace single horizons across larger distances.

4.2. Biostratigraphic correlations

Samples spanning the Sarmatian/Pannonian boundary and samples from units B and C1 were analyzed to test the correlation of the wells. The samples were investigated for foraminifers, ostracods, molluscs and nannofossils. Typical upper Sarmatian assemblages of the *Porosononion granosum* ecobiozone (Papp et al., 1974) have been detected in Rabensburg 2 (710–920 m), Rabensburg 10 (1000 m), Rabensburg 11 (1202–1580 m), Spannberg 2 (880 and 1000 m), Spannberg 21 (866 m), Pirawarth 003 (725, 730 m), Pirawarth 005 (765 m), Zwerndorf 004 (1010 m), Aderklaa 78 (1250 m) and Mannsdorf 1 (1075 m). Deutschwagram 2 (830 m) yielded mollusc assemblages with *Mohrensternia*, which is characteristic for lower Sarmatian strata (Papp et al., 1974; Harzhauser and Piller, 2004a, 2004b). Ostracod assemblages with Pannonian Cytherideidae and Candonidae were detected in Aderklaa 78 (820 m), Deutschwagram 002 (725 m), Rabensburg 10 (730 m) and Mannsdorf 1 (820–950 m). Pannonian lymnocardiid bivalves were recorded from Matzen 109 (690 m) and Schönkirchen 233 (545 m) and Pannonian molluscs (e.g., *Pisidium* sp., *Parvidacna*? *viennense* (Papp, 1953) and *Pontodreissena minima* (Andrusov, 1900)) derive from Rabensburg 10 (730 m). The investigated nannofossil assemblages are generally dominated by rare and poorly preserved specimens, which were reworked from Cretaceous and/or Paleocene to middle Miocene strata; e.g., the Cretaceous *Micula staurophora* (Gardet, 1955) Stradner, 1963 was recorded in Bo 17 (1180–1195 m), Ma 109 (690–695 m), Schö 50 (549 m). Autochthonous nannofossils are rarely preserved. Dw 2 (510–516 m) and DwK 3 (725–730 m) yield the endemic *Praenoelaerhabdus banatensis* Mihajlovic, 1993, which is indicative for an early Pannonian age (Marunteanu, 1997; Botka et al., 2019).

The cross-correlation of these samples allows to trace the Sarmatian/Pannonian boundary in most of the investigated wells and supports the correlation of the lower Pannonian units in the investigated well as shown in Figs. 3–6.

5. Discussion

5.1. From depth domain to time domain

Harzhauser et al. (2004) correlated the letter zones of Papp (1951) with several wells of the Vienna Basin (including well Eichhorn 1) and established a subdivision based on well log patterns (Fig. 9). Lirer et al. (2009) performed an astronomical tuning of the Badenian, Sarmatian and Pannonian successions of the Eichhorn 1 well (Fig. 9). The tuning of Lirer et al. (2009) derived an age of 11.42 Ma for the Sarmatian/Pannonian boundary in well Eichhorn 1. This is seemingly in contradiction to the 11.6 ma age of this boundary proposed by Vasiliev et al. (2010), ter Borgh et al. (2013) and Magyar (2021). Unit A, which represents the lowermost Pannonian deposits in the VB, comprises coarse siliciclastics in channel fills. Therefore, sedimentation across the Sarmatian/Pannonian boundary was obviously not continuous in the VB. In consequence, the age derived by Lirer et al. (2009) would fit assuming a hiatus of about 200 kyr at the position of well Eichhorn 1. This assumption fits to the fact that the shale line unit B attains only 110 m in Eichhorn 1 but is more than 250 m thicker in the wells of the southern VB, which would easily allow to “accommodate” the missing 200 kyr. Nevertheless, a clear caveat of the solution by Lirer et al. (2009) is the lack of magnetostratigraphic tie-points.

Table 1
Thicknesses of all units in the investigates wells (in m) and estimated duration (in kyr) according to the age model of Lirer et al. (2009). 1: Bernhardsthal-Rabensburg field, 2: Paltendorf field, 3: Spannberg field, 4: Pirawarth field, 5: Bockflieβ field, 6: Matzen field, 7: Aderklaa field, 8: Schwechat field.

Unit	hydrocarb. field	1	1	1	1	1	1	2	2	2	2	3	3	3	4	4	4	6	5
		Bernhardsthal 6	Bernhardsthal 7	Bernhardsthal 5	Rabensburg 2	Rabensburg 10	Rabensburg 11	Eichhorn 1	Paltendorf 1	Paltendorf T1	Ringelsdorf 2	Pirawarth 4	Pirawarth 3	Pirawarth 4	Spannberg 2	Spannberg 8	Spannberg 21	Prottes 8	Bockflieβ 7
	Duration (kyr)	Be6	Be7	Be5	Rab 2	Rab 10	Rab 11	Eich 1	Palt 1	PaltT1	Ring 2	Pir 4	Pir 3	Pir 5	Sp2	Sp8	Sp21	Pr8	Bo7
B	120	34	30	25	0	0	98	113	78	63		18	37	57	48	67	53	72	95
C1	160	149	147	129	121	67	123	147	117	102	110	107	111	122	110	136	94	129	160
C2	90	63	69	79	69	62	67	54	51	45	42	46	42	40	82	79	72	55	62
C3	60	21	22	21	51	29	31	37	42	47	78	49	38	51	23	46	43	42	35
C4	70	44	46	55	49	26	32	53	43	54	67	32	36	32	36	33	38	29	28
C5	60	34	40	41	31	53	39	56	44	53	28	44	45	43	54	58	66	48	64
C6	90	36	41	54	34	31	28	30	32	27	25	43	47	39	47	44	49	41	42
C7	40	25	26	30	14	23	33	22	29	31	26	29	24	25	34	25	29	35	44
D1	90	41	31	46	36	30	34	23	25	28	29	46	42	44	43	39	27	27	22
D2	70	45	46	45	65	52	55	58	76	62	79	27	27	31	26	26	28	26	39
E1	60	19	21	26	28	39	76	47	54	39	52	33	36	37	47	50	49	32	40
E2	70	69	70	69	61	70	73	50	51	50	49	51		52	53	66	55	54	54
E3	50	59	60	64	35	32	31	42	27	38	15	22		43	47	47	42		52
E4	90	51	49	46	61	41	52	53	43	54	51	49		54		38	53		38
F1	60					82	83	64	71	62	58	47					85		60
F2	90					73	102	55	38	34	47						45		
F3	100						68	56	35	30	33								
G1	no data						87		64	66	56								
G2	no data						93		75	83	70								
G3	no data								30		70								

Unit	hydrocarb. field	5	5	6	6	6	6	6	6	6	6	7	7	7	7	8	8	8	8
		Bockflieβ 15	Bockflieβ 17	Schönkirchen 50	Matzen 303	Matzen 126	Schönkirchen 233	Matzen 109	Deutschwagram 2	Deutschwagram K3	Strasshof 2	Aderklaa 78	Kagran 7	Raasdorf 1	Breitenlee 1	Rutzendorf 1	Wittau 1	Mannsdorf 1	Schwechat 1
	Duration (kyr)	Bo15	Bo17	Schö 50	Ma303	Ma126	Schö233	Ma109	Dw2	DwK3	Str 2	Ad78	Ka7	Ra1	Br1	Ru1	Wi1	Ma1	Schw1
B	120	72	83	81	68	47	103	162	71	34	68	143	265	313	304	268	134	243	405
C1	160	163	168	123	154	223	122	173	195	123	262	181	143	147	134	142	262	231	157
C2	90	47	52	47	72	56	53	67	44	26	59	70	62	67	68	74	48	55	77
C3	60	52	52	43	47	27	37	52	54	56	42	66	64	43	36	41	38	40	34
C4	70	22	23	32	27	53	39	38	30	33	32	36	29	40	39	34	30	37	38
C5	60	34	34	41	42	35	36	46	35	52	48	34	55	32	34	46	66	43	33
C6	90	42	46	44	43	38	33	41	40	35	38	52	38	32	35	31	33	28	38
C7	40	44	44	28	28	22	42	38	32	31	45	22	21	32	23	37	30	28	46
D1	90	27	28	24	42	29	23	42	48	58	59	24	19	37	42	46	52	49	40
D2	70	32	32	34		21	22	28	21	42	22	33	34	31	41	39	45	50	32
E1	60	52	58	51		37	43	53	41		28	49	61	48	60	51	52	52	24
E2	70	23	24			32		33	28		39	62	37	27	25	35	29	28	38
E3	50	54	53			52			46		49	42	41	42	44	37	31	21	52
E4	90	39	47			44			52			38	46			61	55	36	48
F1	60	62	69			64			49				51			38	43	48	61
F2	90								36									52	

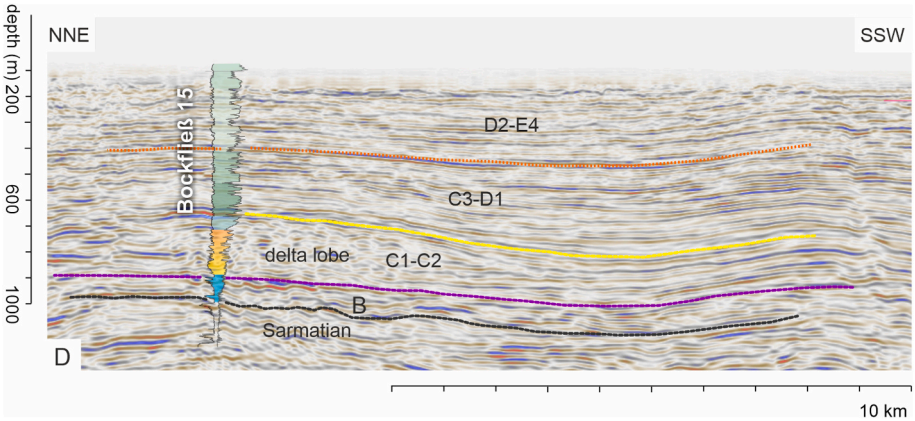

Fig. 8. Seismic data of Pannonian strata in the Bockflieβ field. See line D in Fig. 1 for position.

Herein we correlated the letter units of Harzhauser et al. (2004) with the model of Lirer et al. (2009) (Fig. 9) to derive calculations of sedimentation rates based on the thickness of each unit in each well (Table 1). Applying the model of Lirer et al. (2009) results in following durations: B = 120 kyr, C1 = 160 kyr, C2 = 90 kyr, C3–C5 = 190 kyr, C6–D1 = 220 kyr, D2 = 70 kyr, E1–E2 = 130 kyr, E3–E4 = 140 kyr, F1–F2 = 150 kyr, F3 = 100 kyr. For unit G we cannot deduce such relation because we do not know the time hidden in the gap within this unit as discussed by Harzhauser et al. (2004).

Paleomagnetic data for the Pannonian of the VB are available only for well Spannberg 21, situated at the Spannberg Ridge in the central VB (Paulissen et al., 2011). The data have been acquired onsite during downhole magnetostratigraphic measurements. Paulissen et al. (2011) identified the Sarmatian/Pannonian boundary in well Spannberg 21 at 866 m based on biostratigraphic data, which is confirmed herein. Paulissen et al. (2011) provided a magnetostratigraphy of the well and correlated the Sarmatian/Pannonian boundary with 11.6 Ma. This age of the Sarmatian/Pannonian boundary is in perfect agreement with data by Vasiliev et al. (2010) and ter Borgh et al. (2013) and was also listed by Magyar (2021) in his synthesis on the Pannonian stage and by Borzi et al. (2022) in their discussion on the Paleo-Danube delta. The herein presented cross-correlations, however, question the magnetostratigraphic data of Paulissen et al. (2011).

The basal Pannonian unit B is represented in well Spannberg 21 by an about 50-m-thick sequence. Our cross-correlation suggests that this succession corresponds to the uppermost part of unit B, which is overlain by the Paleo-Danube lobes of unit C1. Consequently, the equivalent of the about 250-m-thick lower part of units B and A, as documented herein from the southern wells, is entirely missing in Spannberg 21. Thus, well Spannberg 21 is an unlikely candidate to cover a continuous Sarmatian/Pannonian boundary. Using the model of Paulissen et al. (2011) would also result in unrealistically low sedimentation rates, which range around 0.3 m/kyr for units C1, C2, E1–E2, around 0.2 for unit E3-E4 and would even drop below 0.2 for unit D2 (asterisk in Fig. 10).

Another problem of the model of Paulissen et al. (2011) is the age of about 9.0 Ma for the uppermost parts of the Pannonian strata in Spannberg 21 (unit F3). At that time, the northern shelf-margin of Lake Pannon was already established in the southern Danube Basin (Magyar et al., 2013), whereas the VB was isolated from Lake Pannon (Harzhauser et al., 2004). In consequence, a difference of 1.1 Ma appears for the uppermost beds in Spannberg 21 when the model of Paulissen et al. (2011) is compared to the proposed age of units F2/F3 derived from the model of Lirer et al. (2009). Furthermore, the model of Paulissen et al. (2011) would require correlating the deposits of unit F with the Turolian Mammal Zone 10, but the unit F mammal faunas of Götzendorf and Stixneusiedl belong to the Vallesian Mammal Zone 9 (Daxner-Höck and Höck, 2015). In consequence, we doubt that the magnetostratigraphy of the Spannberg 21 well can be reliably correlated with the astronomically tuned polarity time scale. We emphasize, however, that Paulissen et al. (2011) did not have information from other wells and could not correlate Spannberg 21 with other records as done herein.

5.2. *Sediment thickness: influence of paleo-topography*

The variability of thickness of the individual units, expressed as standard deviation from the mean, ranges around 12 m for units C2 to G2 but is much higher for units B (97 m) and C1 (43 m) (Fig. 11). This striking variation in thickness of unit B suggests that it fills a paleo-relief of about 300 m, which was successively flooded during the initial phase of Lake Pannon. This interpretation is in agreement with the absence of unit A in many northern wells (Fig. 7B). The shallow northern VB provided only little accommodation aside from the Paltendorf region, where subsidence along the Steinberg Fault generated a slightly deeper zone (Fig. 7B). Similarly, the region around the Spannberg Ridge was relatively shallow. The transition into the deeper basin started in the Aderklaa region and culminated in the Schwechat Depression.

With the termination of unit B, the topography was partly sealed as seen in seismic data, and remaining differences were subsequently balanced by the sand of unit C1. Therefore, unit C1 still shows a NE–SW trend of increasing thickness which, however, is less prominent than in unit B (Fig. 11). In the northern and central VB, unit C1 comprises delta lobes of the Paleo-Danube, which were described and illustrated by Borzi et al. (2022). The subdivision of unit C1 reflects the succession of delta lobe generations overlaying each other (see Borzi et al., 2022; Fig. 4). In the southern wells, unit C1 contains deltaic bodies of yet undefined rivers. A candidate might have been the Paleo-Triesting, which entered the southern VB during the Pannonian (Harzhauser et al., 2004); Wessely (2006). In wells Rabensburg 10, unit C1 directly overlies Sarmatian strata (Fig. 3), pointing to a topographic high in the Rabensburg area. At that time, the Eichhorn-Rabensburg Horst might have formed a small island in Lake Pannon. Such relief is also seen in the Paltendorf field, where unit B is missing in Ringelsdorf 2 but shows an onlap close to Paltendorf T1 (Fig. 7B). The rather uniform thickness of unit C2 suggests that the former topography was now largely sealed and that differences in local subsidence were moderate (Fig. 11). Consequently, in all overlaying units, differences in sediment thickness can be interpreted as differences in regional subsidence rates because changes in the lake level would be reflected by a uniform signal. This interpretation is supported by seismic surveys, which show a rather homogenous, continuous stack of reflectors in the investigation area, with only minor erosional features and comparatively rare clinoforms above C2 (Figs. 7 and 8).

Units C3 to D1 display also a rather uniform distribution (Fig. 8). A slight difference is only visible along the Eichhorn-Rabensburg High with slightly lower subsidence rates during the deposition of units C6–D1. For units D2 to E4, however, a distinct change in subsidence

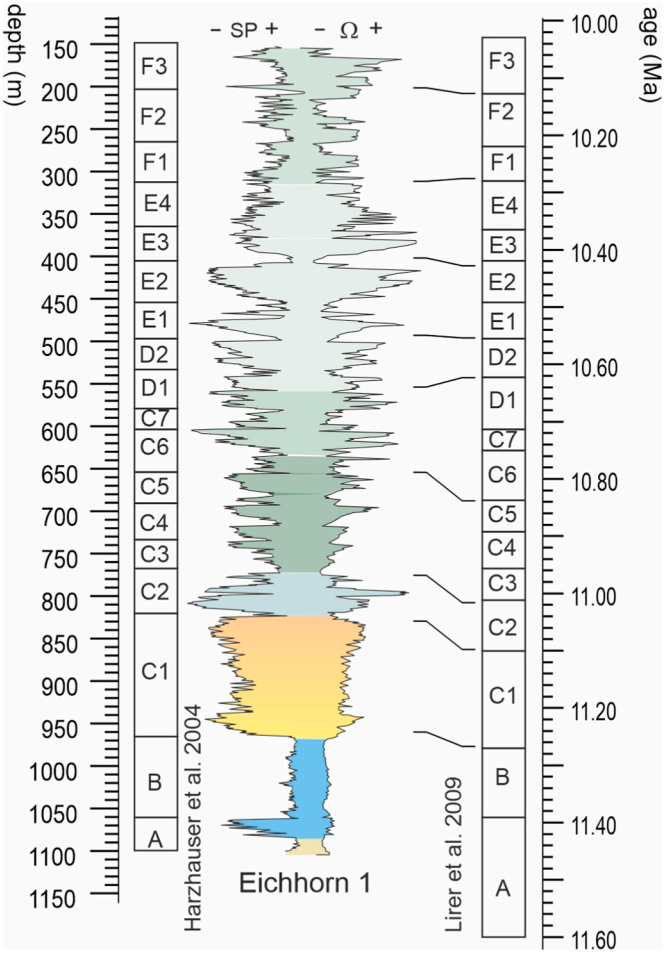

Fig. 9. Correlation the astronomical tuning of well Eichhorn 1 of Lirer et al. (2009) with formations, Pannonian substages as used in the Vienna Basin, and letter units of Harzhauser et al. (2004) established in the same well.

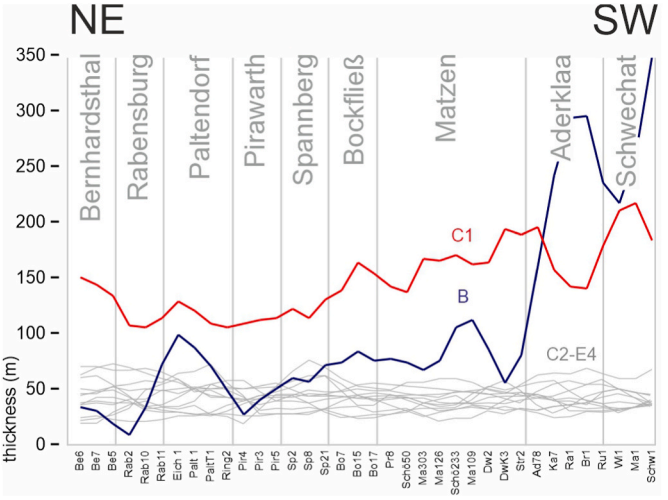

Fig. 11. NE–SW transect of sediment thicknesses through the investigated hydrocarbon fields. Note the striking change between units B and C1 compared to the overlaying units (C2–E4). Units F and G are not shown due to the spotty records.

regime is evident. Now highest subsidence rates occurred in the northern VB in the Bernhardsthal, Rabensburg and Paltendorf fields, whereas sedimentation rates were decreasing in the south (Fig. 10). This trend continued during the formation of units F1 to F3. The overall increase in sedimentation rates was also detected by Hölzel et al. (2008) as "middle Pannonian pulse" (Fig. 12) and explained the coeval subsidence phase in the adjacent Pannonian basins complex.

Thus, the data suggest a northward shift of the depocenter during deposition of the middle Pannonian part of the Bzenec and Cary formations. This successive increase in sedimentation rate, however, does not explain the thick upper Pannonian Gbely Formation in the Rabensburg and Paltendorf fields. Based on the assumption that the entire region was leveled after unit C1, a displacement by faulting of the Bzenec and Cary formations of about 350 m occurred between the Rabensburg 11 and the Paltendorf wells relative to the adjacent

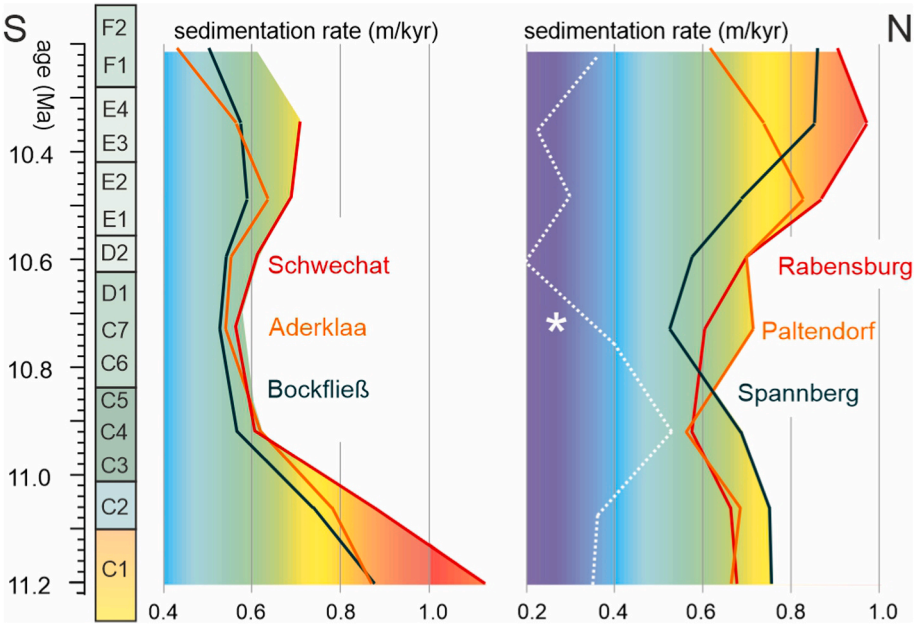

Fig. 10. Sedimentation rates in different hydrocarbon fields (3 point running mean). Asterisk represents hypothetical sedimentation rates in well Spannberg 21 applying the magnetostratigraphy of Paulissen et al. (2011). Note the switch of maximum sedimentation rates from south (Schwechat field) to north (Rabensburg field) through time.

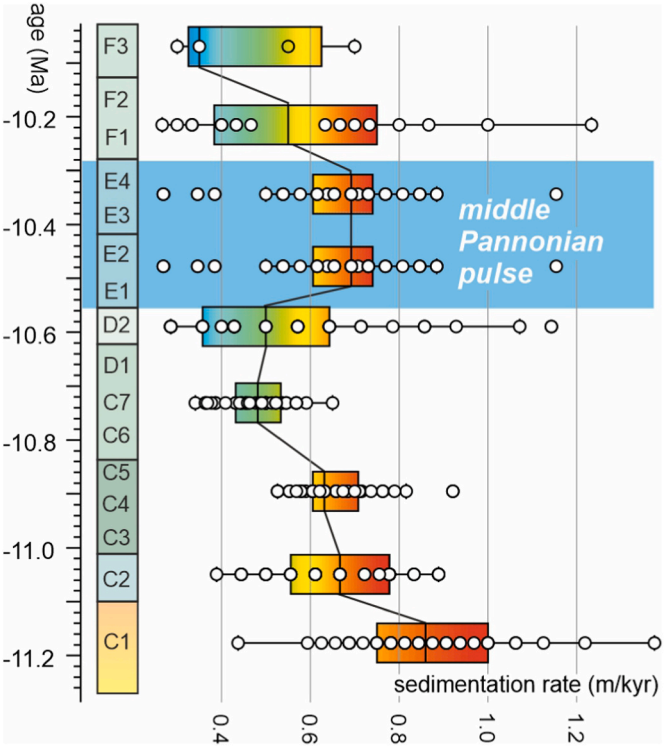

Fig. 12. Box-plots depicting sedimentation rates calculated for all investigated wells, illustrating the middle Pannonian pulse of Hölzel et al. (2008). Note that outliers at the left side are artefacts of incompletely preserved units due to synsedimentary erosion.

Rabensburg and Pirawarth fields. The timing of this displacement postdates the formation of G3.

Our model reveals sedimentation rates of 0.8–1.0 m/kyr for the delta lobes of unit C1 (Fig. 12). Subsequently the sedimentation rate decreased continuously down to 0.5 m/kyr from 11.1 Ma to 10.6 Ma. The sedimentation rate increased afterwards to about 0.7 m from 10.5 to 10.3 Ma. For units E1–E2, this model is in perfect agreement with the sedimentation rates derived by Kern et al. (2012, 2013) for the Hennersdorf core, based on spectral analyses of high resolution data on ostracods and magnetic susceptibility. Subsequently, the sedimentation rate decreased again down to values around 0.5–0.6 m/kyr until 10.1 Ma (Fig. 12).

5.3. Lake level versus sediment input rates versus subsidence

It is tempting to correlate the observed shifts in sedimentation rates with lake level changes and climatic trends. The early Pannonian was characterized a low lake level (Magyar et al., 1999a) and arid conditions (Harzhauser et al., 2007). During the middle Pannonian the lake level was distinctly rising, peaking in its maximum extent during Pannonian Zone E (Magyar et al., 1999a; Neubauer et al., 2016). This ecological trend is reflected by the morphological evolution of certain mollusc lineages (Neubauer et al., 2013) and in the stable isotope record of mollusc shells (Harzhauser et al., 2007). The lake level rise coincided with a strong increase in precipitation in central Europe, which resulted in strongly raised runoff (Böhme et al., 2008, 2011). Therefore, the low sedimentation rates in the lower Pannonian units C2–C7 would correlate with the arid phase, whereas the middle Pannonian rise of sedimentation rates would coincide with increased runoff and a rising lake level.

This interpretation, however, is in conflict with the few available numerical data on lake level changes.

Borzi et al. (2022) performed in-seismic measurements of the clinoforms of the Paleo-Danube delta lobes using true vertical-depth seismic data. These data reveal a minimum lake level of 180 m during the initial phase of the formation of unit C1 and a subsequent decrease of lake water depth down to about 100 m towards the top of C1. This declining water depth caused switches of drainage direction of some of the delta lobes (Borzi et al., 2022) but the declining accommodation is not reflected in the well logs. A major lake level rise of Lake Pannon (mfs 3 between units C2 and C3) caused the flooding of the margins of the VB, resulting in back stepping of fluvial deposits into the North Alpine Foreland Basin, which led to the termination of delta deposition in the VB (Harzhauser et al., 2003; Harzhauser, 2009; Borzi et al., 2022). This event, however, is not reflected by increased sedimentation rates. Thus, we assume that subsidence is the main factor explaining the lateral and temporal shifts in sediment accumulation. Lake level changes, however, are reflected by the observed successions of minor flooding surfaces serrating the funnel-shaped well logs. Thus, the general subsidence signal is modulated by lake level oscillations.

5.4. Do the records provide indications for compression during the Pannonian?

Peresson and Decker (1997a, 1997b) proposed an onset of a compressional tectonic regime in the VB during the late Pannonian, which was adopted in many subsequent schemes depicting the tectonic history of the VB (e.g., Strauss et al., 2006; Lee and Wagreich, 2016, 2017). Their interpretation was based on deformed upper Pannonian strata in the Cary Formation from the Steinfeld outcrop in the southern Vienna Basin (Peresson and Decker, 1997a, 1997b) (corresponding to units F1–F3). This structure, however, was reinterpreted as synsedimentary slump by Exner et al. (2008) and Grundtner et al. (2009). Therefore, the main geological argument for the existence of a compressional regime in the VB during that phase of the late Pannonian was invalidated. The Gbely Formation is the uppermost unit of the Pannonian sediment stack in the VB (comprising the herein studied units G1–G3 and unit H, which is not covered by our data). A late Pannonian age of the Gbely Fm was established based on the mammal fauna, which allows a correlation with the Turolian mammal zones MN 10/11 (Daxner-Höck and Höck, 2015), representing a time span of about 9.6 to 8.0 Ma (Harzhauser et al., 2004). Herein, only 169 m of this formation were drilled in the Paltendorf area but the formation, which seems to be subdivided by two gaps, attains up to 450 m in thickness (Harzhauser et al., 2004). This documents considerable subsidence in the northern VB during the late Pannonian until about 8 Ma. The seismic survey does not reveal any signs of a compressional regime in the upper Pannonian deposits and the fault systems suggest an extensional mechanism (Fig. 7). Especially, the tectonic displacement of units G1–G3 between the Paltendorf region and the adjacent high zones of the Bernhardsthal and Pirawarth areas occurred along a fault after the deposition of the Gbely Formation (see Fig. 7A). This points to ongoing extensional tectonics even after the deposition of the Gbely Formation and is a further argument against a compressional regime during this phase of the Pannonian. Thus, basin inversion occurred at a later stage of basin development. In the adjacent Danube Basin, Šujan et al. (2021) documented the onset of basin inversion around 6 Ma, which would fit to our data and would be in the stratigraphic range proposed by Peresson and Decker (1997a, 1997b) for the VB.

The Gbely Formation (units G1–G3) is preserved only in small graben structures but is missing on the adjacent highs. Thus, the lack of the Gbely Formation in most wells and large parts of the VB documents a post-Pannonian erosion of Upper Miocene strata of about 400 m. This value increases to more than 500 m in areas where also the Cary Formation is missing. This erosion is evidence for the basin inversion discussed by Peresson and Decker (1997a, 1997b) and based on our data, the onset of this basin inversion occurred distinctly after 8 Ma.

6. Conclusions

For the first time, the Pannonian of the Austrian part of the Vienna Basin is correlated along a distance of about 100 km spanning from the hydrocarbon fields in the Bernhardsthal and Rabensburg areas in the NE to the Schwechat Depression in the SE. The investigated well logs display characteristic, laterally repetitive patterns, which allow the separation of distinct sedimentary units, which can be followed along large distances. The basal Pannonian unit displays considerably variability in thickness with a clear NE-SW trend from low to high thickness. This pattern captures the paleo-topography of the VB after the Sarmatian/Pannonian boundary, when basinal marls rapidly filled the deeper parts of the basin. At that time, subsidence was high in the Schwechat Depression but negligible in the northern VB, where the Eichhorn-Rabensburg Horst formed a small island. Thus, the early Pannonian tectonic regime was similar to that of the Sarmatian, when tectonic subsidence was also higher in the southern VB than in the northern VB (Hölzel et al., 2008).

Remnants of the paleo-relief were subsequently filled by the sand of the delta lobes of the Paleo-Danube in the northern and central VB and by other rivers in the Schwechat region. A lake level rise terminated these deltaic developments and a major flooding surface leveled the investigation area. The overlying units C3 to D1 are relatively uniformly developed in the entire investigation area, indicating no marked differences in subsidence in the various hydrocarbon fields. The sedimentation rate was decreasing during this phase from 0.8 to 1.0 m/kyr down to around 0.5 m/kyr (Fig. 12). We consider the latter value to be an estimate of real subsidence, whereas the initial sedimentation rate is rather a matter of the rapidly filled accommodation space of the paleo-relief. Subsequently, sedimentation rates were increasing on average to about 0.7–0.8 m/kyr during the middle Pannonian, which agrees with estimates of Kern et al. (2012, 2013), derived by independent methods. This "middle Pannonian pulse" has also been observed by Hölzel et al. (2008) and was related to the coeval major basin-forming subsidence phase in the adjacent Pannonian basins complex. This pulse, however, was not uniform but was accelerated in the northern part of the VB down to the Spannberg Ridge, whereas subsidence remained constant or decreased in the central and southern VB. The middle Pannonian pulse of subsidence was thus especially related to the Steinberg Fault.

This reveals a threefold Pannonian subsidence history of the Vienna Basin:

- 10.4–11.0 Ma: high subsidence in the southern VB and low subsidence in the northern VB
- 11.0–10.6 Ma: uniform subsidence rates throughout investigation area
- 10.6–10.2 Ma: low subsidence in southern VB and high subsidence in the northern VB

There is no evidence for a decrease of subsidence during the late Pannonian and the faults, displacing the upper Pannonian strata between the Paltendorf region and the adjacent high zones of the Bernhardsthal and Pirawarth areas by about 350 m, suggest persisting extensional tectonics rather than compressional tectonics. Thus, basin inversion occurred after 8 Ma and is reflected by considerably erosion of at least 400 m of uppermost Pannonian deposits. Therefore, a Pannonian compressional regime of the VB is not supported by our data.

Declaration of competing interest

The authors declare that they have no known competing financial interests or personal relationships that could have appeared to influence the work reported in this paper.

Data availability

Data will be made available on request.

Acknowledgments

We thank the OMV Exploration Austria working group, led by Herwig Peresson, for their cooperation.

We acknowledge the support of OMV-AG to provide access to well-log and seismic data to promote geosciences. We thank Jef Deckers (VITO, Belgium) and an anonymous reviewer for their critical but very constructive remarks. Tiago Alves (Cardiff University, UK) is thanked for his guidance and editorial work.

Appendix A. Supplementary data

Supplementary data to this article can be found online at https://doi.org/10.1016/j.marpetgeo.2022.105872.

References

Asquith, G., Krygowski, D., Henderson, S., Hurley, N., 2004. Basic well log analysis. AAPG Methods Explor. 16, 244. https://doi.org/10.1306/Mth16823.

Böhme, M., Ilg, A., Winklhofer, M., 2008. Late Miocene "washhouse" climate in Europe. Earth Planet Sci. Lett. 275, 393–401. https://doi.org/10.1016/j.epsl.2008.09.011.

Böhme, M., Winklhofer, M., Ilg, A., 2011. Miocene precipitation in Europe: temporal trends and spatial gradients. Palaeogeogr. Palaeoclimatol. Palaeoecol. 304, 212–218. https://doi.org/10.1016/j.palaeo.2010.09.028.

Borzi, A., Harzhauser, M., Piller, W.E., Strauss, P., Siedl, W., Dellmour, R., 2022. Late Miocene evolution of the paleo-Danube delta (Vienna Basin, Austria). Global Planet. Change 103769. https://doi.org/10.1016/j.gloplacha.2022.103769.

Botka, D., Magyar, I., Csoma, V., Tóth, E., Šujan, M., Ruszkiczay-Rüdiger, Z., Chyba, A., Braucher, R., Sant, K., Ćorić, S., Baranyi, V., Bakrač, K., Krizmanić, K., Bartha, I.R., Szabó, M., Silye, L., 2019. Integrated stratigraphy of the Guşteriţa clay pit: a key section for the early Pannonian (late Miocene) of the Transylvanian Basin (Romania). Aust. J. Earth Sci. 112, 221–247.

Čtyroký, P., 2000. Nové lithostratigrafické jednotky pannonu videéské pánve na Moravé. Véstnik Ceského Geol. Ustavu 75, 159–170.

Daxner-Höck, G., Höck, E., 2015. Rodentia neogenica. In: Catalogus Fossilium Austriae, vol. 4. Österreichische Akademie der Wissenschaften, Wien, p. 158.

Decker, K., Peresson, H., Hinsch, R., 2005. Active tectonics and quaternary basin formation along the Vienna Basin transform fault. Quat. Sci. Rev. 24, 307–322. https://doi.org/10.1016/j.quascirev.2004.04.012.

Evenick, J.C., 2008. Introduction to Well Logs & Subsurface Maps. PennWell Corporation, Tulsa, p. 236.

Exner, U., Rath, A., Grasemann, B., Draganits, E., 2008. Softsediment deformation and deformation of porous sand: structural highlights in the southern Vienna and Eisenstadt Basin. J. Alpine Geol. 49, 129–136.

Gradstein, F.M., Ogg, J.G., Schmitz, M.D., Ogg, G.M., 2020. The Geologic Time Scale 2020, 2 volumes. Elsevier, Amsterdam, p. 1390. https://doi.org/10.1016/C2020-1-02369-3.

Grundtner, M.L., Harzhauser, M., Mandic, O., Draganits, E., Gier, S., Exner, U., Wagreich, M., 2009. Zur sedimentologie der Sandgrube Steinbrunn (Pannonium, Österreich). Jahrbuch Geol. Bundesanst. 149, 441–451.

Hammer, Ø., Harper, D.A.T., Ryan, P.D., 2001. PAST: paleontological statistics software package for education and data analysis. Palaeontol. Electron. 4 (1), 1–9.

Harzhauser, M., 2009. The Early Vallesian Vertebrates of Atzelsdorf (Late Miocene, Austria). 2. Geology, 111A. Annalen des Naturhistorischen Museums in Wien, pp. 479–488.

Harzhauser, M., Piller, W.E., 2004a. Integrated stratigraphy of the Sarmatian (upper middle Miocene) in the western central paratethys. Stratigraphy 1, 65–86.

Harzhauser, M., Piller, W.E., 2004b. The Early Sarmatian - hidden seesaw changes. Cour. Forschungsinst. Senckenberg 246, 89–112.

Harzhauser, M., Daxner-Höck, G., Piller, W.E., 2004. An integrated stratigraphy of the Pannonian (late Miocene) in the Vienna Basin. Aust. J. Earth Sci. 95/96, 6–19.

Harzhauser, M., Kranner, M., Mandic, O., Strauss, P., Siedl, W., Piller E., W., 2020. Miocene lithostratigraphy of the northern and central Vienna Basin (Austria). Aust. J. Earth Sci. 113, 169–200. https://doi.org/10.17738/ajes.2020.0011.

Harzhauser, M., Latal, C., Piller, W.E., 2007. The stable isotope archive of Lake Pannon as a mirror of Late Miocene climate change. Palaeogeogr. Palaeoclimatol. Palaeoecol. 249, 335–350. https://doi.org/10.1016/j.palaeo.2007.02.006.

Harzhauser, M., Kovar-Eder, J., Nehyba, S., Ströbitzer- Hermann, M., Schwarz, J., Wójcicki, J., Zorn, I., 2003. An early Pannonian (late Miocene) transgression in the northern Vienna Basin. The paleoecological feedback. Geol. Carpathica 54, 41–52.

Hinsch, R., Decker, K., Peresson, H., 2005. 3D seismic interpretation and structural modeling in the Vienna Basin: implication for Miocene to recent kinematics. Aust. J. Earth Sci. 97, 38–50.

Hölzel, M., Wagreich, M., Faber, R., Strauss, P., 2008. Regional subsidence analysis in the Vienna Basin (Austria). Aust. J. Earth Sci. 101, 88–98.

Kern, A.K., Harzhauser, M., Piller, W.E., Mandic, O., Soliman, A., 2012. Strong evidence for the influence of solar cycles on a Late Miocene lake system revealed by biotic and abiotic proxies. Palaeogeogr. Palaeoclimatol. Palaeoecol. 329–330, 124–136. https://doi.org/10.1016/j.palaeo.2012.02.023.

Kern, A.K., Harzhauser, M., Soliman, A., Piller, W.E., Mandic, O., 2013. High-resolution analysis of Upper Miocene lake deposits: evidence for the influence of Gleissberg-band solar forcing. Palaeogeogr. Palaeoclimatol. Palaeoecol. 370, 176–183. https://doi.org/10.1016/j.palaeo.2012.12.005.

Kováč, M., Baráth, I., Kováčová - Slamková, M., Pipík, R., Hlavatý, I., Hudáčková, N., 1998. Late Miocene paleoenvironments and sequence stratigraphy: northern Vienna Basin. Geol. Carpathica 49/6, 445–458.

Kranner, M., Harzhauser, M., Mandic, O., Strauss, P., Siedl, W., Piller, W.E., 2021. Early and middle Miocene paleobathymetry of the Vienna Basin (Austria). Mar. Petrol. Geol. 132, 105187 https://doi.org/10.1016/j.marpetgeo.2021.105187.

Lee, E.Y., Wagreich, M., 2016. 3D visualization of the sedimentary fill and subsidence evolution in the northern and central Vienna Basin (Miocene). Aust. J. Earth Sci. 109/2, 241–251. https://doi.org/10.17738/ajes.2016.0018.

Lee, E.Y., Wagreich, M., 2017. Polyphase tectonic subsidence evolution of the Vienna Basin inferred from quantitative subsidence analysis of the northern and central parts. Int. J. Earth Sci. 106, 687–705. https://doi.org/10.1007/s00531-016-1329-9.

Lirer, F., Harzhauser, M., Pelosi, N., Piller, W.E., Schmid, H.P., Sprovieri, M., 2009. Astronomically forced teleconnection between Paratethyan and Mediterranean sediments during the middle and late Miocene. Palaeogeogr. Palaeoclimatol. Palaeoecol. 275, 1–13. https://doi.org/10.1016/j.palaeo.2009.01.006.

Magyar, I., 2021. Chronostratigraphy of clinothem-filled non-marine basins: Dating the Pannonian stage. Global Planet. Change 205, 103609. https://doi.org/10.1016/j.gloplacha.2021.103609.

Magyar, I., Geary, D.H., Müller, P., 1999a. Paleogeographic evolution of the late Miocene Lake Pannon in central Europe. Palaeogeogr. Palaeoclimatol. Palaeoecol. 147, 151–167.

Magyar, I., Geary, D.H., Sütő-Szentai, M., Müller, P., 1999b. Integrated biostratigraphic, magnetostratigraphic and chronostratigraphic correlations of the Late Miocene Lake Pannon deposits. Acta Geol. Hung. 42/1, 5–31.

Magyar, I., Radivojevic, D., Sztanó, O., Synak, R., Ujszaszi, K., Pócsik, M., 2013. Progradation of the paleo-Danube shelf margin across the Pannonian basin during the late Miocene and early Pliocene. Global Planet. Change 103, 168–173. https://doi.org/10.1016/j.gloplacha.2012.06.007.

Mandic, O., Kurečić, T., Neubauer, T.A., Harzhauser, M., 2015. Stratigraphic and paleogeographic significance of lacustrine molluscs from the Pliocene Viviparus beds in central Croatia. Geol. Croat. 68/3, 179–207. https://doi.org/10.4154/gc.2015.1.

Marunteanu, M., 1997. Evolution line of the endemic genus *Noelaerhabdus* Pannonian; Pannonian basin. Acta Palaeontol. Rom. 1, 96–100.

Neubauer, T.A., Harzhauser, M., Kroh, A., 2013. Phenotypic evolution in a fossil gastropod species lineage: evidence for adaptive radiation? Palaeogeogr. Palaeoclimatol. Palaeoecol. 370, 117–126. https://doi.org/10.1016/j.palaeo.2012.11.025.

Neubauer, T.A., Harzhauser, M., Mandic, O., Kroh, A., Georgopoulou, E., 2016. Evolution, turnovers and spatial variation of the gastropod fauna of the late Miocene biodiversity hotspot Lake Pannon. Palaeogeogr. Palaeoclimatol. Palaeoecol. 442, 84–95. https://doi.org/10.1016/j.palaeo.2015.11.016.

Papp, A., 1951. Das Pannon des Wiener Beckens. Mitt. Geol. Ges. Wien 39, 99–193, 1946-1948.

Papp, A., Marinescu, F., Seneš, J., 1974. M5. Sarmatien (sensu E. Suess, 1866). Die Sarmatische Schichtengruppe und ihr Stratotypus. Chronostratigr. Neostratotypen 4, 1–70.

Paulissen, E., Luthi, S.M., Grunert, P., Ćorić, S., Harzhauser, M., 2011. Integrated high-resolution stratigraphy of a Middle to Late Miocene sedimentary sequence in the central part of the Vienna Basin. Geol. Carpathica 62, 155–169. https://doi.org/10.2478/v10096-011-0013-z.

Peresson, H., Decker, K., 1997a. The tertiary dynamics of the northern Eastern Alps (Austria) changing palaeostresses in a collisional plate boundary. Tectonophysics 272, 125–157. https://doi.org/10.1016/S0040-1951(96)00255-7.

Peresson, H., Decker, K., 1997b. Far-field effects of Late Miocene subduction in the Eastern Carpathians: E-W compression and inversion of structures in the Alpine-Carpathian-Pannonian region. Tectonics 16, 38–56. https://doi.org/10.1029/96TC02730.

Royden, L.H., 1985. The Vienna Basin: a thin-skinned pullapart basin. In: Biddle, K., Christie-Blick, N. (Eds.), Strike Slip Deformation, Basin Formation and Sedimentation, vol. 37. Society of Economics Palaeontologists and Mineralogists Special Publication, pp. 319–338. https://doi.org/10.2110/pec.85.37.0319.

Siedl, W., Strauss, P., Sachsenhofer, R.F., Harzhauser, M., Kuffner, T., Kranner, M., 2020. Revised Badenian (middle Miocene) depositional systems of the Austrian Vienna Basin based on a new sequence stratigraphic framework. Aust. J. Earth Sci. 113, 87–110. https://doi.org/10.17738/ajes.2020.0006.

Strauss, P., Harzhauser, M., Hinsch, R., Wagreich, M., 2006. Sequence stratigraphy in a classic pull-apart basin (Neogene, Vienna Basin). A 3D seismic based integrated approach. Geol. Carpathica 57, 185–197.

Šujan, M., Rybár, S., Kováč, M., Bielik, M., Majcinc, D., Minárd, J., Plašienka, D., Nováková, P., Kotulová, J., 2021. The polyphase rifting and inversion of the Danube Basin revised. Global Planet. Change 196C, 103375. https://doi.org/10.1016/j.gloplacha.2020.103375.

ter Borgh, M., Vasiliev, I., Stoica, M., Knežević, S., Maţenco, L., Krijgsman, W., Rundić, L., Cloetingh, S., 2013. The isolation of the Pannonian basin (Central Paratethys): new constraints from magnetostratigraphy and biostratigraphy. Global Planet. Change 103, 99–118. https://doi.org/10.1016/j.gloplacha.2012.10.001.

Vasiliev, I., de Leeuw, A., Filipescu, S., Krijgsman, W., Kuiper, K., Stoica, M., Briceag, A., 2010. The age of the Sarmatian–Pannonian transition in the transylvanian basin (central Paratethys). Palaeogeogr. Palaeoclimatol. Palaeoecol. 297, 54–69. https://doi.org/10.1016/j.palaeo.2010.07.015.

Wessely, G., 2006. Niederösterreich. Geologie der Österreichischen Bundesländer. Geologische Bundesanstalt Wien, p. 416.